Paper submitted to 21st ASME/AIChE National Heat Transfer Conference
July 24-28, 1983; Seattle, Washington

SOME THERMAL HYDRAULICS ASPECTS OF THE IMPURITY CONTROL SYSTEM FOR FED/INTOR

Y. S. Cha, R. F. Mattas, M. A. Abdou
Argonne National Laboratory
Fusion Power Program
Argonne, Illinois 60439

J. R. Haines
Oak Ridge National Laboratory
Fusion Engineering Design Center
Oak Ridge, Tennessee 37830

July 1983

SOME THERMAL-HYDRAULICS ASPECTS OF THE IMPURITY CONTROL SYSTEM FOR FED/INTOR

Y. S. Cha, R. F. Mattas, M. A. Abdou
Argonne National Laboratory
Fusion Power Program
Argonne, Illinois 60439

J. R. Haines
Oak Ridge National Laboratory
Fusion Engineering Design Center
Oak Ridge, Tennessee 37830

ABSTRACT

This paper addresses two important aspects of thermal-hydraulics related to the design of limiter/divertor of Fusion Engineering Device and International Tokamak Reactor. The results of both analyses provide input to the determination of the lifetime of the limiter/divertor which is the most critical engineering problem for the impurity control system.

The first part of the paper is to provide temperature calculations for the limiter and divertor. Steady-state, two-dimensional, temperature distributions are obtained, through the use of the computer code THTB, for the top surface of the limiter or divertor plate and for the leading edge (cylindrical geometry) of the limiter. Results are reported for various combinations of coating and structural materials. Thermal conductivity and coating thickness are found to be the most important parameters for given surface heat flux distributions. At the leading edge, there are two factors competing with each other when the coating material is relatively thick. The radial reduction in heat transfer area tends to increase the temperature while radiative heat transfer losses at high surface temperature tends to decrease the structural temperature.

The second part of the paper describes the analysis of the tangential motion of a melt layer during plasma disruption. An analytical solution is developed. The results show that fairly large displacement (~ 10 mm) could be reached under nominal conditions. Limitations of this analytical model are discussed and possible improvements are proposed.

NOMENCLATURE

- F body force per unit mass
- t time
- u time independent component of w
- v time dependent component of w
- w melt layer velocity in the z-direction parallel to the solid structure
- x coordinate perpendicular to the solid structure
- z coordinate in the direction parallel to the solid structure
- ℓ melt layer thickness
- ν kinematic viscosity

Superscript * indicates dimensionless quantity

INTRODUCTION

This paper addresses two important aspects of thermal-hydraulics related to the design of the impurity control system (limiter and divertor) of the Fusion Engineering Device (FED) and the International Tokamak Reactor (INTOR). A brief summary of the objectives, history, and development of FED/INTOR can be found in reference (1). The primary purposes of either the poloidal divertor or the pumped-limiter are to exhaust a small amount of helium from the plasma, to remove heat and to provide for an acceptably small level of eroded (from the wall) impurities in the plasma.

The basic configurations of the poloidal divertor and the pumped limiter considered for the FED/INTOR are shown in Figures 1 and 2. The poloidal divertor is located at the bottom of the plasma chamber with a continuous toroidal opening extending around the reactor. The divertor is divided into 12 modules, one for each TF coil. The outer and inner divertor plates are placed at angles of 15° and 30°, respectively, to the separatrix. Both plates are flat with a peak heat flux of 2.4 MW/m^2.

The limiter is located at the bottom of the plasma chamber and extends toroidally around the entire chamber. It is divided into 12 modules to allow removal. The limiter is curved (concave side facing the plasma) with two pumping channels. The limiter is shaped to reduce the peak heat flux on the front surface. A two pumping channel configuration is preferred over the one-channel limiter because, for the same pumping requirements, the heat load on the critical leading edge region can be substantially reduced. The peak heat flux on the leading edge is ~ 1 MW/m^2.

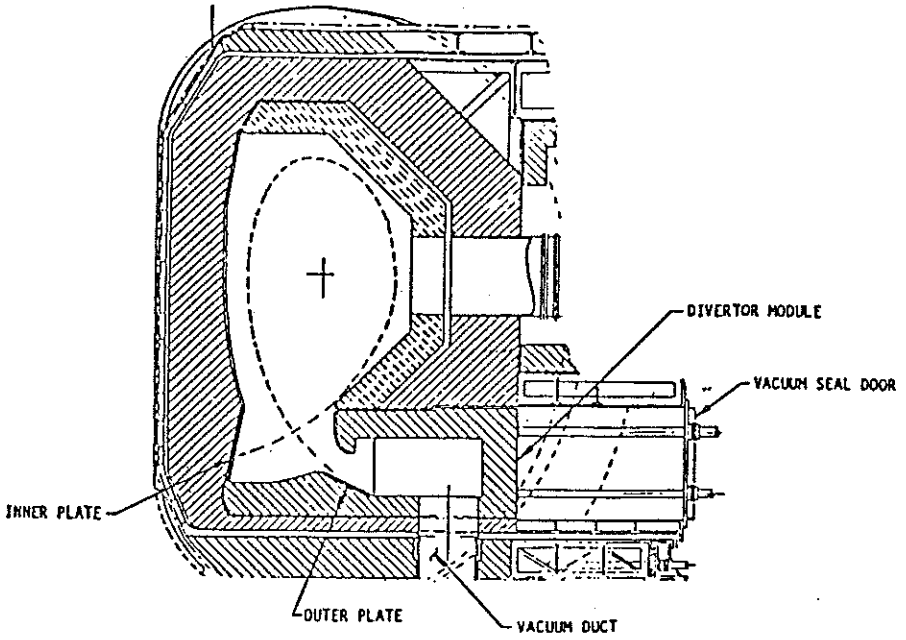

Figure 1. Divertor configuration.

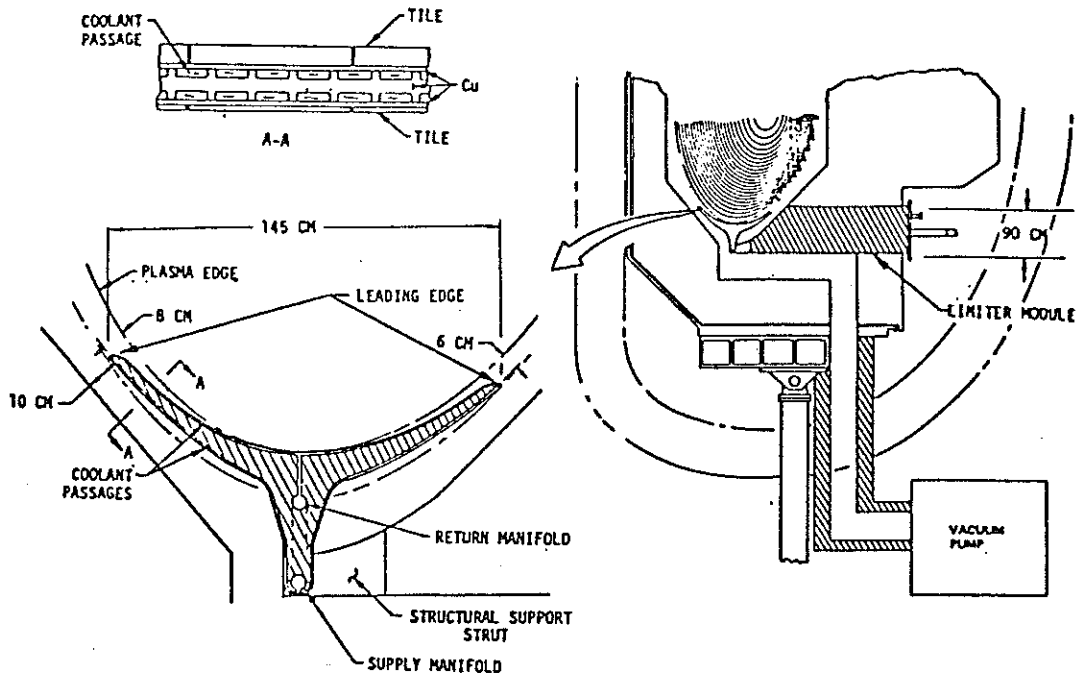

Figure 2. Shaped limiter - bottom (double edge)

The first part of the paper is devoted to the determination of temperature distributions in various combinations of the coating/structural materials proposed for the limiter/divertor of FED/INTOR. Parametric analysis of the reference limiter and the divertor were performed, using an extensive set of material combinations and thicknesses. The results of the temperature distributions are used as input for the stress and fatigue analysis and for the determination of the maximum allowable thicknesses for various materials (1). The second part of the paper describes the analysis of the tangential motion of the melt layer under the influence of magnetic force during plasma disruption. The results of both analyses provide inputs to the determination of the lifetime of the limiter (or divertor) which is the most critical problem for the impurity control system as far as the engineering and materials considerations are concerned (1).

PARAMETRIC ANALYSIS OF LIMITER/DIVERTOR

It is generally recognized that some type of protective coating (surface material) is needed on the plasma side of the limiter/divertor plate. Relatively thick coating may be required in view of the predicted large erosion rate in certain areas of the limiter (1). The attachment of the coating material to the structural (heat sink) material is a critical issue as it greatly influences the performance and the reliability of the design. For the present analysis, a brazed condition is assumed between the coating and structural material. The coating material considered are beryllium (Be), beryllium oxide (BeO), silicon carbide (SiC), and tungsten (W). The structural materials included are a copper alloy (Cu) and a vanadium alloy (V-15Cr-5Ti). The materials and parameters investigated are summarized in Table 1. The surface heat flux distributions are obtained from the plasma engineering calculations and are used as input to the thermal-hydraulic calculations. The thermal contact conductance between the coating and the structural material is assumed to be very large which corresponds to the brazed condition. Bulk nuclear heating for the various materials is also included in the calculations, but except for very thick coatings, the effect is small compared to the fairly large surface heat fluxes. Pressurized water with a velocity of 9.2 m/s is used as the coolant. A heat transfer coefficient of 4×10^4 W/m^2-°C is used for the coolant/structure interface. This value is slightly conservative for a coolant velocity of 9.2 m/s. The material property with the largest uncertainty is the emissivity of the surface material. Radiative heat transfer is particularly important for low conductivity materials, such as SiC and BeO, which are predicted to operate at relatively high temperatures. In the present calculations, an emissivity of 0.5 is assumed for all the coating materials. Radiative heat transfer is assumed to occur between the limiter (or divertor) and the first wall which is at a constant temperature of 300°C. Temperature dependent thermal conductivities are used for both the coating and the structural materials. Thermophysical properties of these materials are adopted from reference (1).

The computer code THTB (2), is used for the parametric analysis. THTB is a 3-dimensional, transient computer code devoted primarily to the temperature calculations of solid structures. The top surface of the limiter or the divertor plate is modelled by a slab geometry and the leading edge of the limiter is modelled by a cylindrical geometry (Fig. 3). Two dimensional, steady-state calculations are performed and the results are described in the following paragraphs.

Figure 4 shows the maximum coating temperature versus coating thickness at the top surface of the limiter (or the divertor plate) for different combinations of coating/structure materials. Similar behaviors were observed for the leading edge of the limiter. Beryllium exhibited lower temperatures as a result of relatively high thermal conductivities. Beryllium oxide has very high thermal conductivity at lower temperatures and the thermal conductivity decreases sharply with increasing temperature. Figure 5 shows the variation of thermal conductivity with temperature for these coating materials. Standard silicon-carbide has the lowest thermal conductivity and therefore exhibited the highest temperature. When the coating temperature is relatively low (< 1000°C), the slope in Figure 4 increases with the coating thickness. As the temperature becomes relatively high (> 1000°C) and increases further with the coating thickness, the slope begins to decrease for SiC-V, SiC-Cu, and BeO-V. This is the result of increased contribution from radiation (from the limiter/divertor to the first wall) heat transfer.

Figure 6 shows the temperature distributions in the coating material as a function of depth in the coating at the top surface for different coating thicknesses of BeO-V and Be-V. For Be-V, the temperature distribution in Be is almost linear (except near the surface) for all thicknesses. This is the result of fairly low beryllium temperatures. For BeO-V, with 10 mm thick coating, the temperature distribution in BeO is also close to linear. For BeO-V with 20 or 30 mm thick coating, the temperature distribution in BeO is non-linear and the gradient increases towards the surface. This is again the result of a sharp reduction in thermal conductivity with temperature for BeO. Similar behaviors were observed for the leading edge of the limiter.

Figure 7 shows the maximum structure (heat sink) temperature vs. coating thickness at the top surface (slab geometry) for different combinations of coating/structure materials. For relatively thin coatings (1 and 10 mm), the structure temperature increases slowly with the coating thickness and the maximum structure temperature is independent of the coating material on the top surface of the limiter or divertor plate. Vanadium is always at higher temperatures than that of copper as a result of relatively poor thermal conductivity of vanadium. When the coating thickness is increased beyond 10 mm, the structure material temperature becomes dependent upon not only the coating thickness, but also the coating material, as shown in Figure 7. This interesting behavior is the result of significant radiative heat transfer from the surface of the limiter/divertor to the first wall. The structural material temperature depends mainly on the surface heat flux, the thermal conductivity, and the thickness of the structural material. An increase in radiative heat transfer at high surface temperatures is equivalent to a net reduction in surface heat flux which in turn reduces the temperature of the structural material. This is why the temperatures of both vanadium and copper decrease with coating thickness for the cases of BeO and SiC when the coating is relatively thick. For the

Table 1. Materials and Parameters Examined for the Limiter/Divertor

Heat Flux:	2.4 MW/m^2 uniform for top surface; 1.0 MW/m^2 maximum for the leading edge and decreases linearly to zero at the back of the leading edge.
Coating Material:	Beryllium (Be), Silicon-Carbide (SiC), Beryllium Oxide (BeO), and Tungsten (W).
Coating Thickness:	1, 10, 20, and 30 mm.
Structural Material:	Copper Alloy (Cu) and Vanadium Alloy (V) (1.5 mm thick).
Emissivity:	~ 0.5 (BeO and SiC).
Bulk Nuclear Heating: (W/cm^3)	7.8 (Be), ~ 7.8 (BeO and SiC), 23 (W), 14.7 (Cu), and 7.4 (V).
Coating/Structure Interface Conductance:	Very large.
Structure/Coolant Heat Transfer Coefficient:	$4.0 \times 10^4 \frac{W}{m^2-{}^0C}$
Coolant Inlet Temp:	60°C.
Coolant Average Velocity:	9.2 m/s

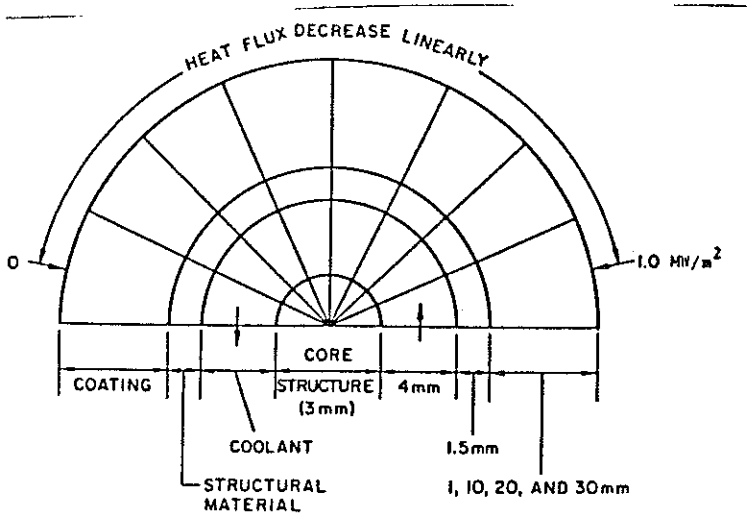

Fig. 3. Geometry of the leading edge used for temperature calculations.

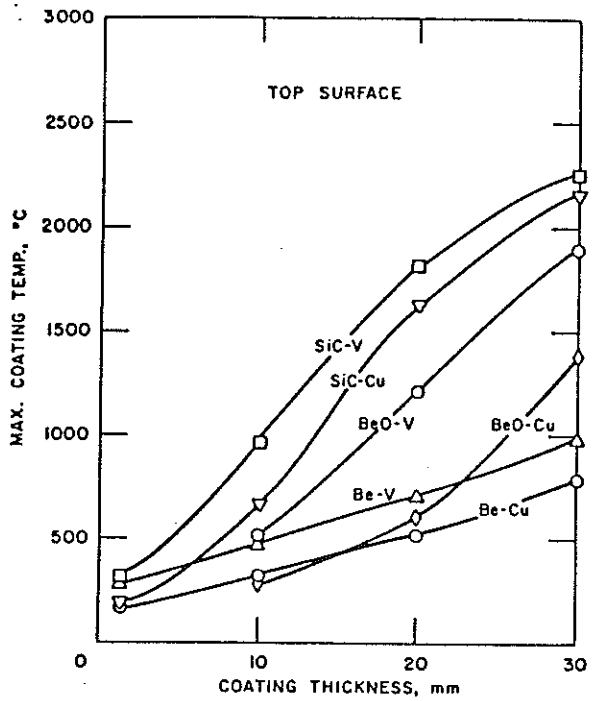

Fig. 4. Maximum coating temperature versus coating thickness for various coating/structure material combinations in the top surface of a limiter or divertor plate.

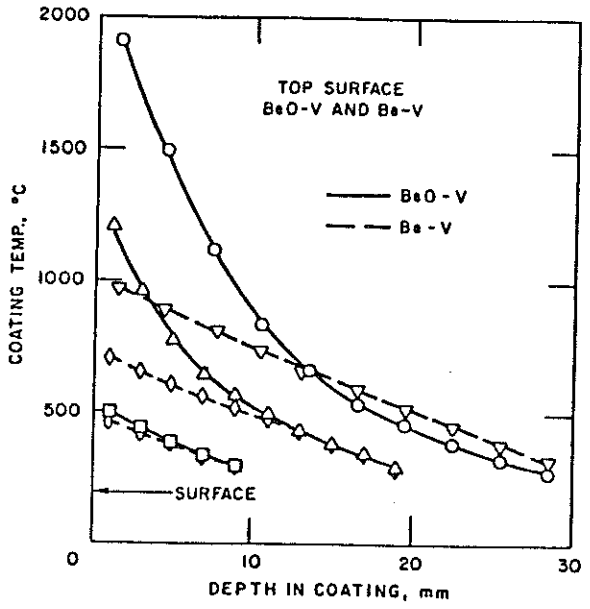

Fig. 6. Temperature profile for the coating material in the top surface of a limiter or divertor plate.

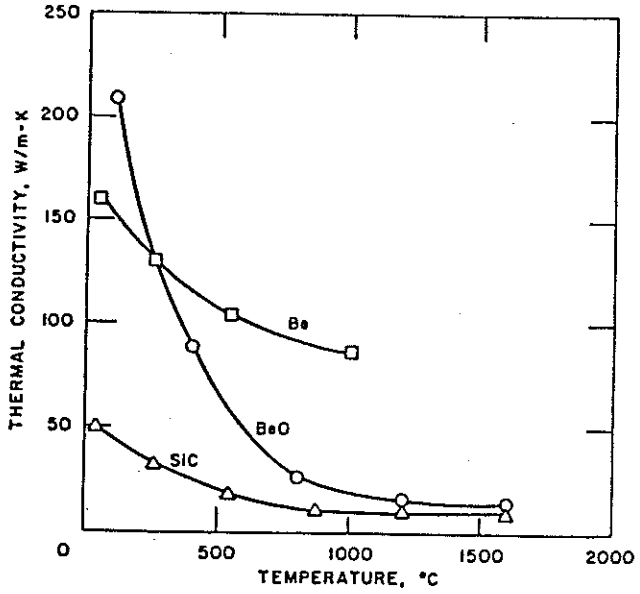

Fig. 5. Conductivity versus temperature for various coating materials.

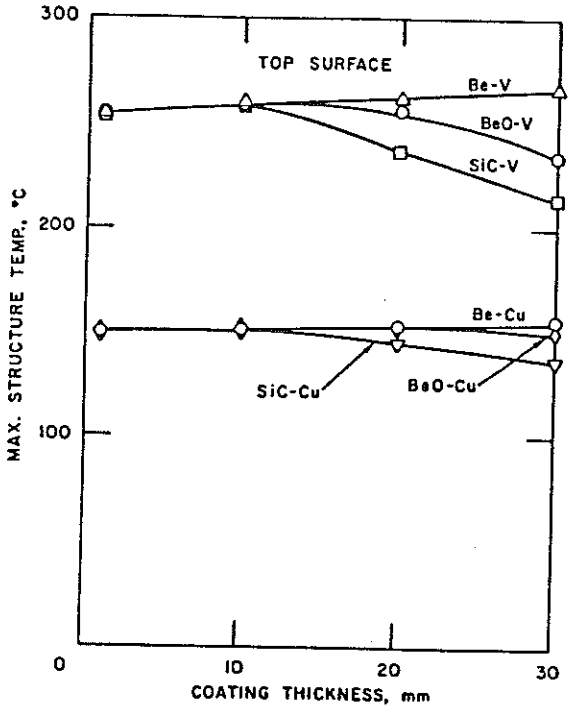

Fig. 7. Maximum heat sink temperatures as a function of surface coating thickness.

case of beryllium, radiative heat transfer is not significant even with a very thick coating, therefore, the temperature of the structural material beneath beryllium does not decrease with coating thickness.

The temperature distributions in all the structural materials were found to be linear for both the top surface of the limiter or the divertor plate and the leading edge of the limiter. This is expected since the structural material is always at fairly low temperature and thickness is small (1.5 mm). Vanadium has a much higher temperature gradient than that of copper because copper has a higher conductivity than vanadium.

Figure 8 shows the maximum structure temperature vs. coating thickness for various combinations of coating/structure materials at the leading edge. The temperature behavior of the structural material at the leading edge is quite different from the temperature behavior at the top surface. First, for relatively thin coatings (< 10 mm), there is a sharp increase in structural material temperature with increasing coating thickness. This is the result of reduction in heat transfer area radially from the coating inward towards the coolant at the leading edge. This geometry effect does not exist at the top surface of the limiter where the structural temperature remains nearly constant with coating thickness. As the coating thickness is increased further, the previously described effect of radiative heat transfer becomes important for BeO-V, SiC-V, and SiC-Cu. At the leading edge, there are two factors competing with each other when the coating is thick (temperature is high). The radial reduction in heat transfer area tends to increase the temperature, while radiative heat transfer losses at high surface temperatures tends to decrease the structural temperatures. Figure 8 indicates that the effect of reduction in heat transfer area is controlling at high temperatures (thick coatings) and the structural temperature continues to increase with coating thickness at the leading edge.

Figure 9 shows the comparison of the maximum temperature in the coating and structural materials between the top surface and the leading edge of the limiter for SiC-V. Up to a coating thickness of 30 mm, the maximum coating temperature in the leading edge is always less than that of the top surface as a result of lower surface heat flux at the leading edge. This is not the case for the structural material. For relatively thin coating material (< 10 mm), the maximum structural temperature in the top surface is greater than that at the leading edge. As the coating thickness is increased beyond 10 mm, the trend is reversed, i.e., the maximum structural temperature in top surface is less than that at the leading edge. These results are typical of all materials for the surface heat fluxes distribution assumed in the calculations.

TANGENTIAL MOTION OF MELT LAYER DURING PLASMA DISRUPTION

It is predicted by several models (3,4) that formation of a melt layer on the surface of the limiter (or divertor) is very likely during plasma disruption as a result of relatively large energy density and short disruption time. The thickness of the melt layer varies with time and depends mainly on the material of the limiter (or first wall) and the

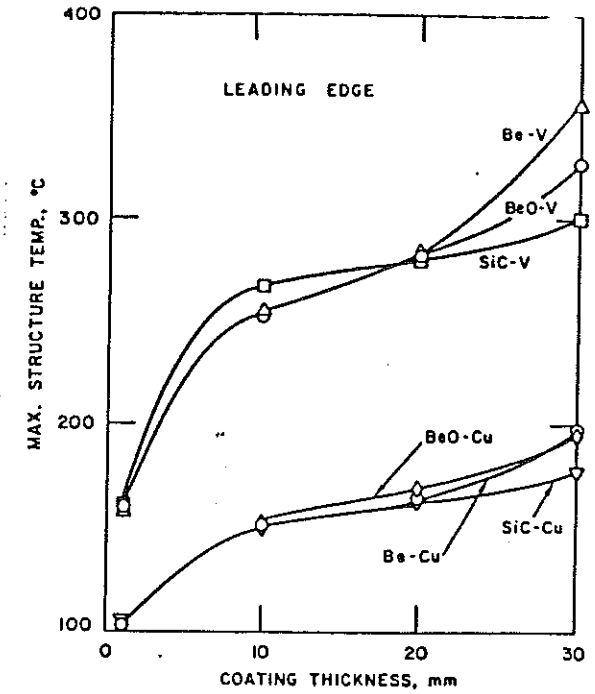

Fig. 8. Maximum structural temperatures at the leading edge as a function of surface material thickness for several surface materials.

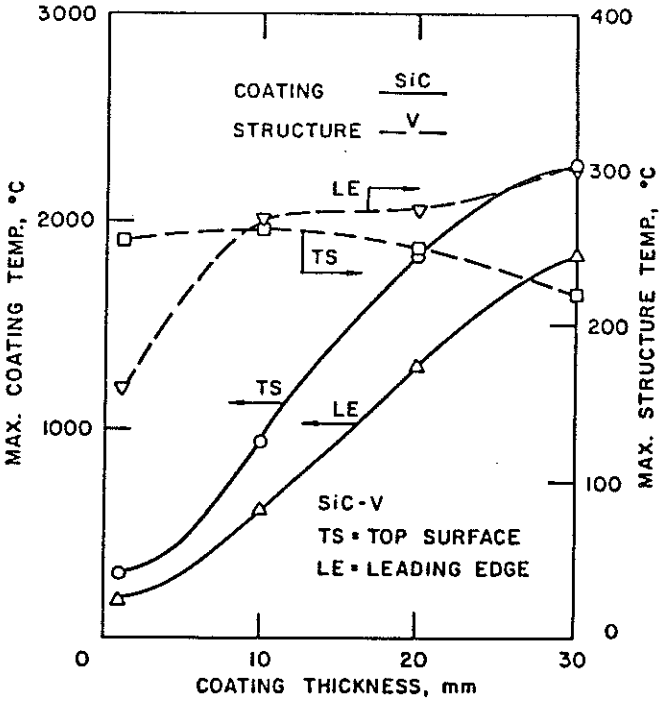

Fig. 9. Comparison of the maximum temperature versus coating thickness for the limiter top surface and leading edge.

postulated disruption characteristics (disruption period, peak energy density). During a disruption, a number of driving forces may cause the melt layer to move. These forces include gravitational, electromagnetic, ablation (impulsive), etc. These driving forces act against the inertia, surface tension, and viscous forces of the melt layer. The consequence can be quite different for different forces and the melt layer would move in directions either normal or parallel to the solid structure. It is important to examine the extent of the melt layer movement under the influence of various driving forces and determining which is the dominating mechanism.

The objective of this paper is to provide a simplified analysis of the tangential motion of the melt layer under the influence of body force so that the results can be compared with other modes of motion to determine which is the most critical with regard to the life time of the impurity control system. As a first approximation, we shall limit the analysis to a melt layer with constant thickness, constant temperature and thermophysical properties, under the action of constant body force. The geometry and the coordinate system used in the analytical model is shown in Figure 10. The melt layer is assumed to have a thickness of ℓ and the body force (F) is parallel to the interface between the melt layer and solid structure. The body force can either be gravity or magnetic force. To further simplify the analysis, we assume that the motion is one-dimensional, and the melt layer velocity (w) in the z direction is a function of x only ($\frac{d}{dz} = 0$).

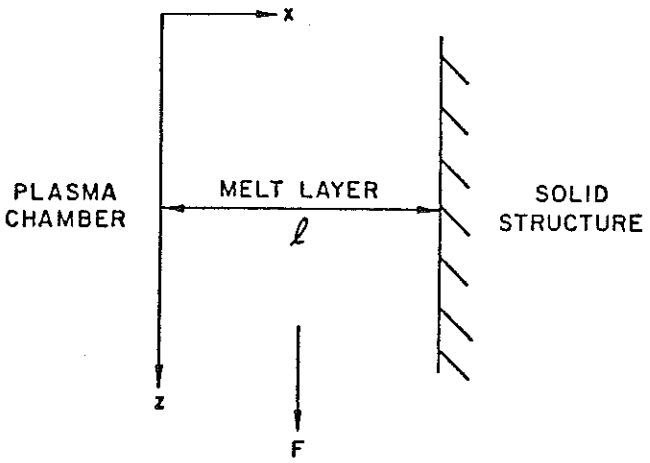

Fig. 10. Geometry and coordinate system for the melt layer.

The thickness (ℓ), the body force per unit mass (F), and the kinematic viscosity (ν) of the melt layer are assumed to be constants. The equation of motion in the z direction is

$$\frac{dw}{dt} = F + \nu \frac{d^2w}{dx^2} \tag{1}$$

Eq. (1) is a balance among inertia, body, and viscous forces of the melt layer. The initial and boundary conditions are:

$$\left.\begin{aligned} w(o,x) &= 0 \\ w(t,\ell) &= 0 \\ \left(\frac{dw}{dx}\right)_{x=0} &= 0 \end{aligned}\right\} \tag{2}$$

In Eq. (2), we have assumed that the melt layer is initially at rest and that the interface between the melt layer and the plasma is a free surface.

Following the method described in (5), we let

$$w(t,x) = u(x) + v(t,x) \tag{3}$$

Substituting Eq. (3) into Eqs. (1) and (2), resulted in the following sets of equations:

$$\left.\begin{aligned} \nu \frac{d^2u}{dx^2} &= -F \\ u(\ell) &= 0 \\ \left(\frac{du}{dx}\right)_{x=0} &= 0 \end{aligned}\right\} \tag{4}$$

and

$$\left.\begin{aligned} \frac{dv}{dt} &= \nu \frac{d^2v}{dx^2} \\ v(o,x) &= -u(x) \\ v(t,\ell) &= 0 \\ \left(\frac{dv}{dx}\right)_{x=0} &= 0 \end{aligned}\right\} \tag{5}$$

Direct integration of Equation (4) gives

$$u = \frac{F}{2\nu}(\ell^2 - x^2) \tag{6}$$

The solution to Eq. (5) with u given by Eq. (6) can be obtained from (5)

$$v = \frac{2F\ell^2}{\nu} \sum_{\eta=0}^{\infty} \exp(-\nu B^2 t/\ell^2) \left[\frac{\cos(B)}{B^2} - \frac{\sin(B)}{B^3}\right] \cos\left(\frac{Bx}{\ell}\right) \tag{7}$$

where $B = (2\eta + 1)\pi/2$

Introducing the following dimensionless parameters,

$$w^* = \frac{w\nu}{F\ell^2}$$

$$x^* = x/\ell$$

$$t^* = t\nu/\ell^2$$

and substituting Eqs. (6) and (7) into Eq. (3),

$$w^* = (1 - x^{*2})/2 + 2 \sum_{\eta=0}^{\infty} \exp(-t^* B^2) \left[\frac{\cos B}{B^2} - \frac{\sin B}{B^3}\right] \cos Bx^* \tag{8}$$

Eq. (8) is the complete solution to Eqs. (1) and (2) in dimensionless form. It can be seen from Eq. (8) that w^* has a steady-state component and a transient component. As t becomes very large, the transient component vanishes and

$$w^* \simeq (1 - x^{*2})/2 \qquad \text{As } t^* \to \infty$$

The dimensionless maximum velocity in the melt layer occurs at the free surface ($x = 0$) and has a magnitude of 0.5.

Figure 11 is the plot of dimensionless velocity versus dimensionless distance at various dimensionless time calculated by using Eq. (8). It can be observed from Figure 11 that the melt layer velocity profile gradually approaches some steady-state value and that the maximum velocity always occurs at the free surface at any instant. The results shown in Figure 11 is general and applies to any material (liquid), body force, and thickness. For specific applications, one needs the values of F, ν, and ℓ to calculate the velocity and displacement of the melt layer. Since uncertainties exist regarding the values of these variables (particularly F and ℓ) during a disruption, parametrical studies using a range of values for these variables are adequate at this time. A typical calculated melt layer thickness is of the order of 0.1 mm (4). Kinematic viscosity for liquid metals typically range from 10^{-6} m^2/s to 10^{-7} m^2/s. The largest uncertainty appears to be associated with the magnetic force in the direction parallel to the solid structure. The magnetic force in the direction normal to the solid structure is known to be fairly large (~ 100 times gravity, see reference (1)). Not only the magnitude of this magnetic force changes with time, it also reverses its direction during a disruption. In this study, a nominal value of 20 g is selected for the magnetic force parallel to the solid structure. Figure 12 shows the velocity profiles of a melt layer with nominal values of F, ν, and ℓ, over a period of 30 ms. A melt layer usually exists over a period comparable to that of the disruption (5 ms or 20 ms). After this period, the melt layer completely solidifies. The key issue is then to determine whether there is enough time for the melt layer to attain sufficiently high velocities and cause significant displacement of the material on the surface of the limiter or the first wall. Figure 12 indicates that under nominal conditions, the velocities near the free surface of the melt layer are likely to reach, say, magnitude of one meter per second.

Of particular interest is the displacement of the melt layer up to a particular instant during a disruption. The displacement at any location can be obtained by integrating the velocity with respect to time. Figures 13 to 15 show the maximum displacement (at the free surface) of the melt layer versus disruption time for various values of body force, melt layer thickness, and kinematic viscosity. Figure 13 shows that the maximum displacement increases strongly with the magnitude of the body force. As shown in Figure 13 the melt layer is under the influence of gravity only (F = 1 g), the maximum displacement is about 1 mm even near the end of a disruption (t = 20 ms). This kind of displacement is probably acceptable. However, if magnetic forces are present and have a magnitude significantly higher than gravity (for example, F = 20 g), the maximum displacement can reach as high as 10 or 20 mm during a disruption. Figure 14 shows the effect of viscosity on the movement of the melt layer. It can be observed that the displacement increases with decreasing viscosity. Figure 15 shows the effect of melt layer thickness on the displacement. It is obvious that the thicker the melt layer, the larger the displacement at any instant during a disruption.

It should be noted that the results of the analytical model can only be used in a qualitative sense for trend indication. There are several major limitations of the analytical model. The first limitation is that the magnetic force is not constant and varies with time. This limitation can be removed by developing a numerical model and the variation of the magnetic force with time can easily be incorporated. Such a model is curently being developed. The second limitation is that the thickness of the melt layer does not remain constant during a disruption. This limitation can also be removed by discretizing the thickness (obtained from plasma-wall interaction calculations during a disruption) at each time step in the numerical model.

SUMMARY

The results of the parametric analysis of the limiter/divertor is summarized below followed by a summary of the melt layer analysis.

1. Both structural materials, V and Cu, exhibited fairly low temperatures (Cu < 200°C and V < 360°C) and are acceptable under the assumed operating conditions shown in Table 1.

2. SiC and BeO have poor thermal conductivities at medium and high temperatures which resulted in much higher coating temperatures compared to Be with the same thickness. However, this does not imply that Be is preferred over SiC and BeO since both SiC and BeO have much higher melting points than Be. Criteria for determining the maximum acceptable coating temperatures are numerous (melting point, swelling and creep induced by radiation, vaporization temperature, chemical sputtering temperature, etc.) and a detailed account of those parameters on the life-time of the limiter/divertor can be found in reference (1).

3. At high coating temperatures (which correspond to thick coating materials), radiative heat transfer becomes important which resulted in the reduction of structure material temperature with increasing coating thickness in the top surface. At the leading edge, the effect of reduction in heat transfer area radially is controlling, which resulted in a sharp increase in structural temperature with coating thickness when it it relatively thin (< 10 mm) and a gradual increase with coating thickness at thicknesses where radiative heat transfer becomes significant.

4. For the assumed surface heat flux distributions, the coating temperature in the top surface is always greater than that at the leading edge. This statement is also valid regarding the temperature of the structural material when the coating is thin (< 10 mm). However, when the coating thickness further increases, the temperature of the structural material at the leading edge becomes greater than that of the structural material at top surface and condition at the leading edge becomes controlling.

5. The temperature gradients in the coating materials remain fairly constant in both the top surface and leading edge in the radial direction when the coating temperature is fairly low. The temperature profiles become non-linear when the

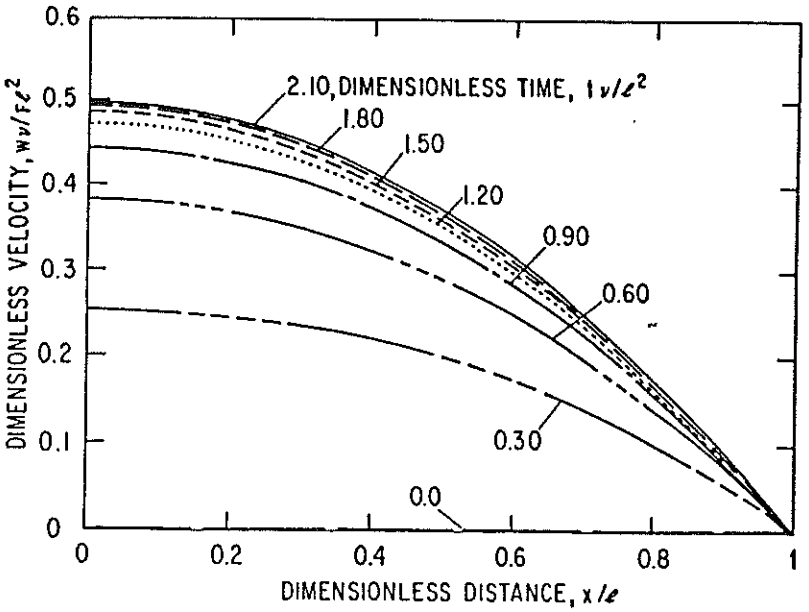

Fig. 11. Dimensionless velocity versus dimensionless distance for various values of dimensionless time.

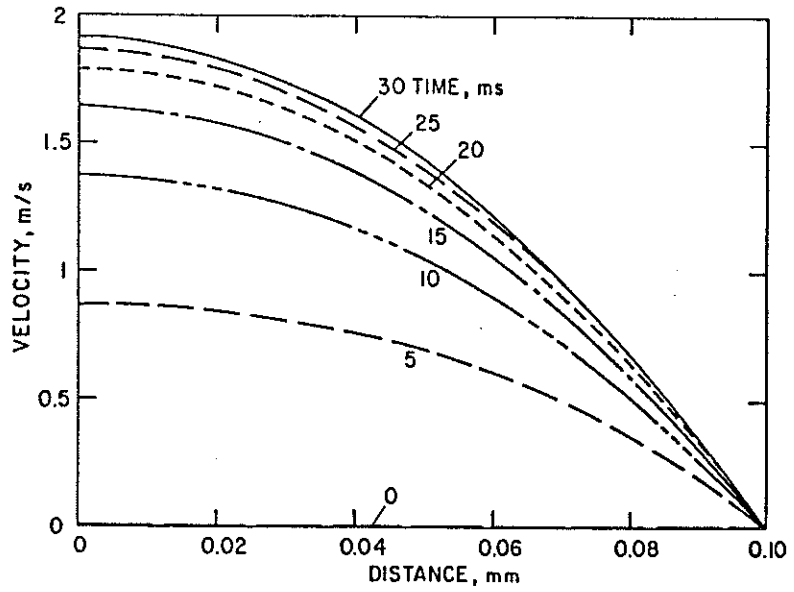

Fig. 12, Velocity profiles of the melt layer at various times for F = 20 g, $\nu = 5 \times 10^{-7}$ m^2/s, and $\ell = 10^{-4}$m.

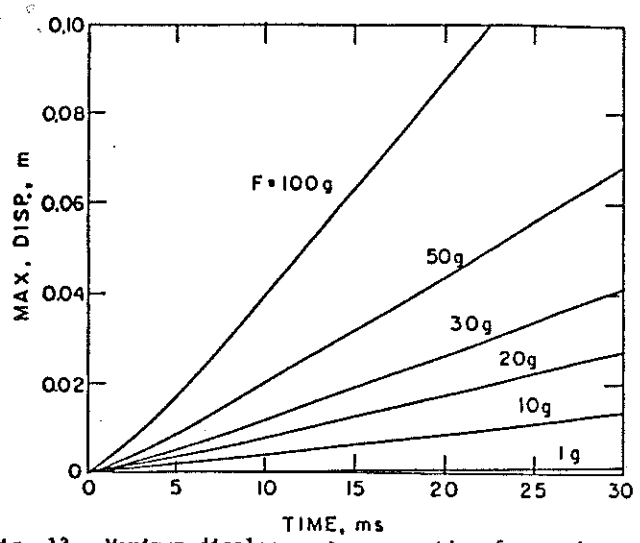

Fig. 13. Maximum displacement versus time for various values of body force with $\nu = 10^{-6}$ m^2/s, and $\ell = 10^{-4}$ m.

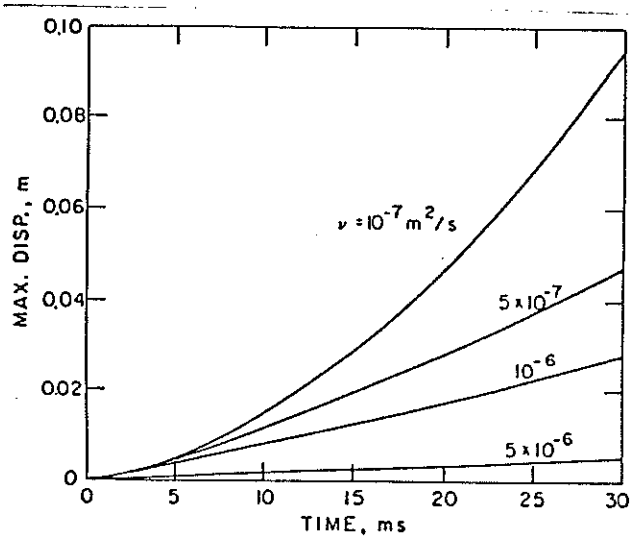

Fig. 14. Maximum displacement versus time for various values of kinematic viscosity with F = 20 g, and $\ell = 10^{-4}$ m.

coating temperature is high (very thick coating). The temperature profiles in the structural materials are always linear as a result of the relatively low temperature and small thickness (1.5 mm) of the structural material. At the leading edge, the radial temperature is always larger than the circumferential temperature gradient.

6. An analytic solution is developed for the tangential motion of a melt layer on the surface of a limiter/divertor during plasma disruption. The results show that under nominal conditions, the maximum velocity in a melt layer can reach ~ 1 m/s at the end of a disruption (30 ms). The maximum displacement can reach a magnitude of ~ 10 mm which may have a significant impact on the lifetime of the limiter/divertor.

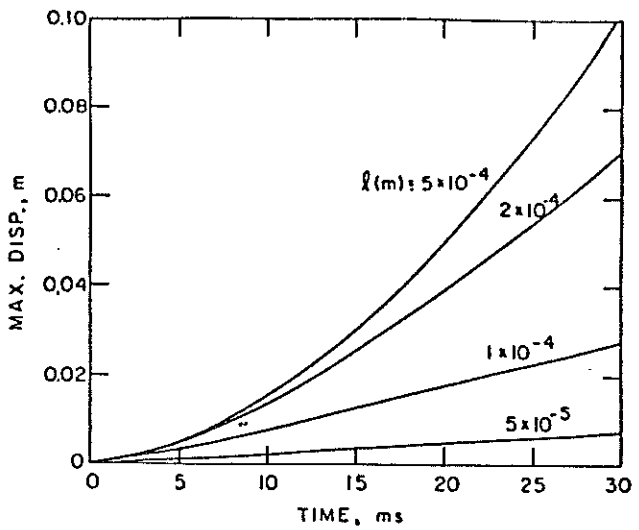

Fig. 15. Maximum displacement versus time for various values of melt layer thickness with F = 20 g, and $\nu = 10^{-6}$ m^2/s.

7. The closed-form solution developed for the tangential motion of the melt layer is limited to constant body force and constant melt-layer thickness, therefore, the results can only be viewed in a qualitative sense. These restrictions can be relaxed by developing a numerical solution for the motion of the melt layer, which should predict more accurately the velocities and displacements than the simplified analytical solution.

REFERENCES

1. M. A. Abdou, et al., "Impurity Control and First Wall Engineering," Chapter VII of U.S. FED-INTOR Activity and The U.S. Contribution to the International Tokamak Reactor, Phase-2A Workshop, Vienna, Austria, IAEA, USA FED-INTOR/82-1 (1982).

2. G. L. Stevens and D. J. Campbell, "Program THTB for Analysis of General Transient Heat Transfer Systems," General Electric Technical Information Series No. R60FPD 647, 1961.

3. B. Merrill, Plasma Disruption, Impurity Control and First Wall Engineering, USA Input to INTOR Workshop, Session III, Phase 2A, FED-INTOR/ICFW/81-02, December, 1981.

4. A. M. Hassanein, G. L. Kulcinski, and W. G. Wolfer, "Dynamics of Melting, Evaporation, and Resolidification of Materials Exposed to Plasma Disruptions," Paper presented at the Fifth International Conference on Plasma Surface Interaction in Controlled Fusion Devices, May, 1982, Gatlinburg, TN.

5. H. S. Carslaw and J. C. Jaeger, Conduction of Heat in Solids, Oxford University Press, 1959.